JACS
JOURNAL OF THE AMERICAN CHEMICAL SOCIETY

Article

pubs.acs.org/JACS

Kinetically Controlled Nucleation of Silver on Surfactant-Free Gold Seeds

Kyle D. Gilroy, Robert A. Hughes, and Svetlana Neretina*

College of Engineering, Temple University, Philadelphia, Pennsylvania 19122, United States

Supporting Information

ABSTRACT: We report on the heterogeneous nucleation of Ag on Au seeds using a surfactant-free synthesis where nanoparticle aggregation is nullified through the immobilization of bare Au seeds on the surface of a substrate. Requiring only silver nitrate, ascorbic acid, and Au seeds, the synthesis is facile and, from a mechanistic standpoint, far less convoluted than conventional protocols. The results reveal that, even in the absence of surfactants, highly anisotropic growth modes are achieved which result in a lone Ag structure emanating from a single (100) Au facet. Consistent with surfactant-based protocols is the ability to vary the product of the reaction by varying the reaction rate. It allows for kinetic control which is able to direct the reaction toward either a bimetallic heterodimer or a core−shell configuration. The observed growth modes cannot be explained in terms of those proposed for surfactant-based growth modes where surfactants, surface diffusion, and/or collision patterns are used to rationalize the reaction product. We, instead, propose a growth mode reliant on the formation of a space charge region around each seed consisting of a double layer of ions, where the integrity of the layer is dependent upon the facets expressed by the seed, the rate at which the reduced ions are being deposited, and the pH of the solution. Our work reveals the rich nature of surfactant-free heteroepitaxial growth modes as well as the utility of the substrate-based platform in defining growth pathways.

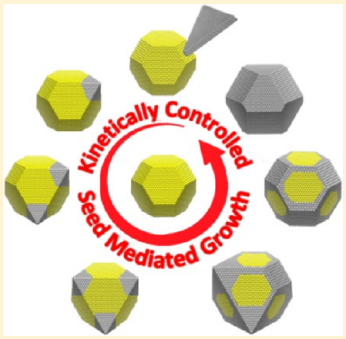

INTRODUCTION

The seed-mediated synthesis of metallic nanostructures in liquid media has given rise to an extraordinary range of nanomaterials with functionalities resulting from the ability to tailor the size, shape, and composition of the structure.[1,2] Extending synthetic protocols beyond single-component systems to the realm of bimetallic nanostructures offers the opportunity to create architectures with enhanced functionalities derived from the integration of materials with dissimilar physical and chemical properties into a single nanostructure.[3] Such structures have already attracted considerable attention due to their potential for application in the areas of catalysis,[4−8] plasmonics,[9,10] chemical and biological detection,[11−13] and magnetism.[14] The full potential of such structures will, however, only be realized if a new set of synthetic challenges associated with heterogeneous nucleation, maintaining heteroepitaxy, and controlling a facet-dependent overgrowth are overcome.

With the potential for attaining important catalytic and plasmonic properties, seed-mediated strategies present a compelling route for the synthesis of bimetallic noble metal nanostructures with a core−shell morphology (denoted as core@shell). While a number of early synthetic achievements were reported for the Au@Ag system,[15−18] the protocol of Sanedrin et al.[19] is unique in their demonstration of L-ascorbic acid (AA) as an effective agent capable of uniformly reducing Au^{3+} ions onto Ag seeds. Using the same reducing agent, Habas et al.[20] demonstrated the formation of Pt@Pd structures where Pd deposited conformally on well-faceted Pt seeds. Their attempts to form Pt@Au structures, however, resulted in anisotropic growth modes, a result which led them to conclude that the poor morphology was associated with the sizable lattice-mismatch occurring at the Au−Pt interface (4.08% compared to 0.7% for Pd−Pt). In a comparative study, Fan et al.[21] used AA to reduce Ag, Pd, and Pt onto Au seeds with an octahedron geometry. While conformal epitaxial overgrowth was observed for the Au@Ag and Au@Pd systems, the Pt overgrowth of the Au seed was both rough and polycrystalline. With the Au@Pd system showing conformal epitaxial growth and the largest lattice-mismatch (i.e., larger than Au@Pt), the work demonstrated that epitaxial heterogeneous nucleation was not simply dependent on having a small lattice-mismatch. On the basis of these results, they proposed three criteria for epitaxial heterogeneous nucleation: (i) the lattice constant of the shell metal should be less than that of the core where the degree of mismatch is less than 5%; (ii) the electronegativity of the shell metal should be less than that of the core metal; and (iii) the bond energies between the core and shell atoms should be larger than those between shell atoms. The motivation behind the criteria was to promote conditions analogous to those used to achieve smooth heteroepitaxial film growth in the vapor phase (i.e., a Frank−van der Merwe growth mode) while preventing the galvanic replacement of the metal seed. It is, however, noted that Qin and co-workers[22] showed that the galvanic replacement of Ag nanocubes could be augmented by

Received: August 8, 2014
Published: October 6, 2014

   dx.doi.org/10.1021/ja5081635 | J. Am. Chem. Soc. 2014, 136, 15337−15345

an AA-induced co-reduction of Au and Ag onto the corners and edges of the cube. Their synthesis yielded hollow Au−Ag nanocubes with sharpened geometrical features and an enhanced Ag content, properties which gave rise to a 33-fold improvement in the surface-enhanced Raman scattering. By increasing the deposition rate through the use of a strong reducing agent, they were also able to completely block the galvanic replacement of Ag and, thus, form Ag@Au nanocubes.[23]

An even more thorough understanding began to emerge with the demonstration of the decisive role that kinetics play in determining the reaction product. Using the Pt@Pd system, Lee et al.[24] demonstrated, through modulations to the reduction rate, that it was possible to transform the growth mode from one where Pd overgrew the {100} facets of a Pt nanocube to one where the Pd growth emanated from multiple corners of the cube. Using the same system, Lim et al.[25] varied the rate of reduction through the use of strong and weak reducing agents (i.e., AA vs citric acid) and conclusively demonstrated that faster kinetics gave rise to conformal deposition while a slower rate of reaction resulted in dimer structures. Yang et al.[26] observed similar behavior and used it to assert kinetic control over the reduction of Ag onto Au seeds in a manner yielding an impressive family of intricate bimetallic nanostructures. Recently, Zhu et al.[27] performed a detailed study on the Pd@Ag system where they explored numerous aspects of the reaction including the concentration of both the shelling and seed material, the molecular weight of the capping layer, the strength of the reductant, the pH, and the reaction temperature. They showed that the conformal overgrowth of a Pd seed with Ag occurred when (i) the capping layer, polyvinylpyrrolidone, had a higher molecular weight and a lower concentration, (ii) the reductant was stronger (i.e., hydrazine vs formaldehyde), and (iii) the reaction was carried out at a higher temperature. While these important findings all point toward the seed-mediated synthesis of bimetallic nanostructures being heavily reliant on reaction kinetics, the exact mechanisms responsible for such phenomena are still under consideration.[28]

Taken together, the aforementioned studies demonstrate that the seed-mediated synthesis of bimetallic nanostructures is sensitive to a wide range of parameters including temperature, pH, the surfactant utilized, the strength of the reducing agent, the precursor concentration, injection rates, the physical properties of the seed (i.e., size, shape, faceting, composition), and seed−shell interfacial interactions arising from differences in lattice constant, electronegativity, and bond energies. While such sensitivities lead to a high degree of synthetic flexibility, the highly intertwined nature of these parameters makes it difficult to decipher growth pathways and determine if particular parameters are acting synergistically or in discordance. The role of surfactants is particularly convoluted as they can (i) prevent nanoparticle aggregation,[29] (ii) induce anisotropic growth modes through preferential binding to specific facets,[30] (iii) act as effective reducing agents able to generate solution-based nanostructures (i.e., the polyol process),[31] and/or (iv) induce plating of a secondary metal onto a preformed seed.[32] Synthetic routes carried out in a surfactant-free environment are, therefore, compelling from the standpoint of establishing a mechanistic framework as they allow for chemical interactions at the seed−solution interface which are defined purely by the intrinsic surface energy of the expressed seed facets against the chemical potential of the solution.

The synthesis of bimetallic core−shell structures using surfactant-free protocols is often impractical when using solution-dispersed seeds because there is a strong tendency for both the seeds and the forming structures to aggregate. This tendency to aggregate can, however, be nullified if the seeds are immobilized on the surface of a substrate. Previously, we demonstrated the utility of this approach in the synthesis of substrate-based hollow metal nanoshells and nanocages using galvanic replacement reactions.[33−35] In addition to eliminating the surfactant requirement, the substrate-based platform offers a number of other advantages including the ability to (i) form nanostructures in periodic arrays, (ii) easily assemble a wide variety of seed materials using solid-state dewetting[36] and associated techniques,[37,38] (iii) control the crystallographic orientation of the seed through its heteroepitaxial relationship with the underlying substrate, and (iv) form faceted seeds which take on a truncated octahedron geometry which exhibits distinct {100} and {111} facets.[39] Herein, we utilize this platform to investigate the heterogeneous nucleation of Ag on surfactant-free Au seeds. The nucleation event is investigated from start to finish for three kinetic regimes where for each case Au seeds are examined which have their [100], [110], or [111] axis perpendicular to the surface of the substrate. The study demonstrates both a facile synthesis route for the generation of a distinct family of substrate-based core−shell structures while providing insights into the underlying kinetic mechanisms which modulate the seed-mediated synthesis of bimetallic nanostructures in an aqueous medium.

EXPERIMENTAL SECTION

Chemicals and Materials. Au and Sb sputter targets were cut from 0.5 mm thick foils with 99.99+% purity (Alfa Aesar) and 99.999% pure rods (ESPI Metals), respectively. The (0001)-oriented sapphire substrates with areal dimensions of 1 × 1 cm^2 were cleaved from 3 in. diameter polished wafers (MTI Corp.). Au seeds were assembled in ultrahigh purity Ar. Silver nitrate ($AgNO_3$) with 99.9999% purity and L-ascorbic acid with 99.0% purity were purchased from Sigma-Aldrich. Deionized (DI) water with a resistivity of 18.2 MΩ·cm was used for the preparation of all aqueous solutions. Glassware was cleaned with aqua regia and thoroughly rinsed in DI water. All chemicals were used as received.

Synthesis of Nanomaterials. Substrate-based Au seeds were prepared on (0001)-oriented sapphire as randomly positioned structures with a wide size distribution and as periodic arrays of similarly sized structures. For the random structures, a 17 nm thick film of Au was sputter deposited onto a 12 nm thick sacrificial layer of Sb whose sublimation at high temperatures enhances the dewetting process.[38] The samples were heated to 1100 °C in ultrahigh purity Ar and then cooled to room temperature over the course of a few hours. This heating regimen causes the film to agglomerate into isolated islands which then melt and recrystallize as the temperature is decreased. The periodic arrays were prepared using a lithography-free technique which we describe in detail elsewhere.[37] The resulting Au seeds showed a high degree of size uniformity (Supporting Information, Figure S1) and were predominantly [111]-oriented, but where seeds with other orientations were also available for characterization. The solution-based overgrowth of these seeds with Ag was carried out for three kinetic regimes referred to as slow, moderate, and fast. For the slow regime, substrate-immobilized Au seeds were placed in a 4 mL aqueous solution of 100 mM $AgNO_3$ which was preheated to 100 °C. The substrate temperature was then allowed to equilibrate for 5 min, after which Ag was reduced onto the Au seeds through the dropwise injection of 1 mL of 1 mM AA every 2 s for approximately 2 min (30 μL/s) followed by a dwell time of 8 min

dx.doi.org/10.1021/ja5081635 | J. Am. Chem. Soc. 2014, 136, 15337−15345

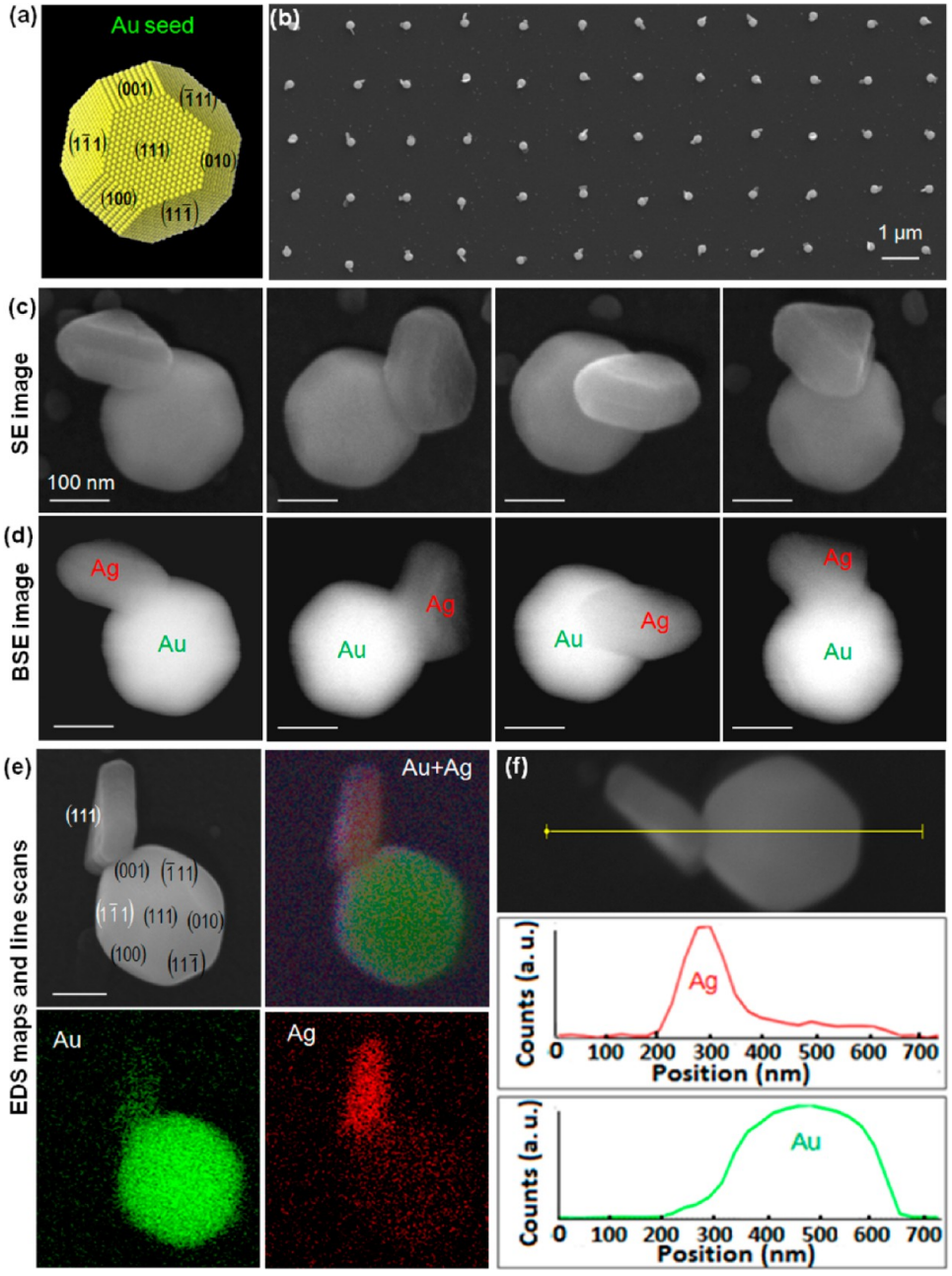

Figure 1. Morphological and elemental characterization of Au–Ag heterodimer structures formed in the regime of slow kinetics. (a) Schematic depicting the expected topography for a [111]-oriented Au seed with facets defined by the geometry of a truncated octahedron. (b) SEM image of a periodic array of Au–Ag dimer structures. High-magnification SEM images of individual structures taken in (c) secondary electron (SE) and (d) backscattered electron (BSE) mode. (e) Elemental maps and (f) line scans showing the distribution of Au and Ag within the dimer structure.

before substrate removal. Growth on the Au seeds was accompanied by the unwanted spontaneous nucleation of solution-based Ag nanostructures, many of which adhered to the surface of the substrate. In fact, most of the Ag is consumed by such spontaneous nucleation events. After the reaction, the substrate was removed from the beaker and immediately placed in an ultrasonic bath of DI water for 2 min, a procedure which proved to be effective in removing most of the unwanted structures. The substrate was then removed from the beaker and dried in a flow of compressed air. The moderate regime utilized the same concentrations of $AgNO_3$ and AA, but where a fast injection of AA (500 μL/s) was used followed by a dwell time of 10 min before substrate removal. In certain instances, the dwell time was reduced or extended to observe the structure at an earlier or later stage of the reaction. The fast regime utilized 100 mM $AgNO_3$ followed by the fast injection of 100 mM of AA. The Au seeds, which appeared red in color, were transformed by these syntheses to red-orange, orange-white, or white depending on whether low, moderate, or high concentrations were used.

Instrumentation. Au and Sb depositions were carried out using a model 681 Gatan high-resolution ion beam coater. The seed assembly process was carried out in a Lindberg Blue M tube furnace. Scanning electron microscopy (SEM), energy-dispersive X-ray spectroscopy (EDS), and elemental maps were obtained using an FEI 450 FEG ESEM.

RESULTS AND DISCUSSION

Bimetallic Structures Synthesized in the Regime of Slow Kinetics. A highly anisotropic growth mode is observed when [111]-oriented Au seeds with a truncated octahedron

dx.doi.org/10.1021/ja5081635 | J. Am. Chem. Soc. 2014, 136, 15337–15345

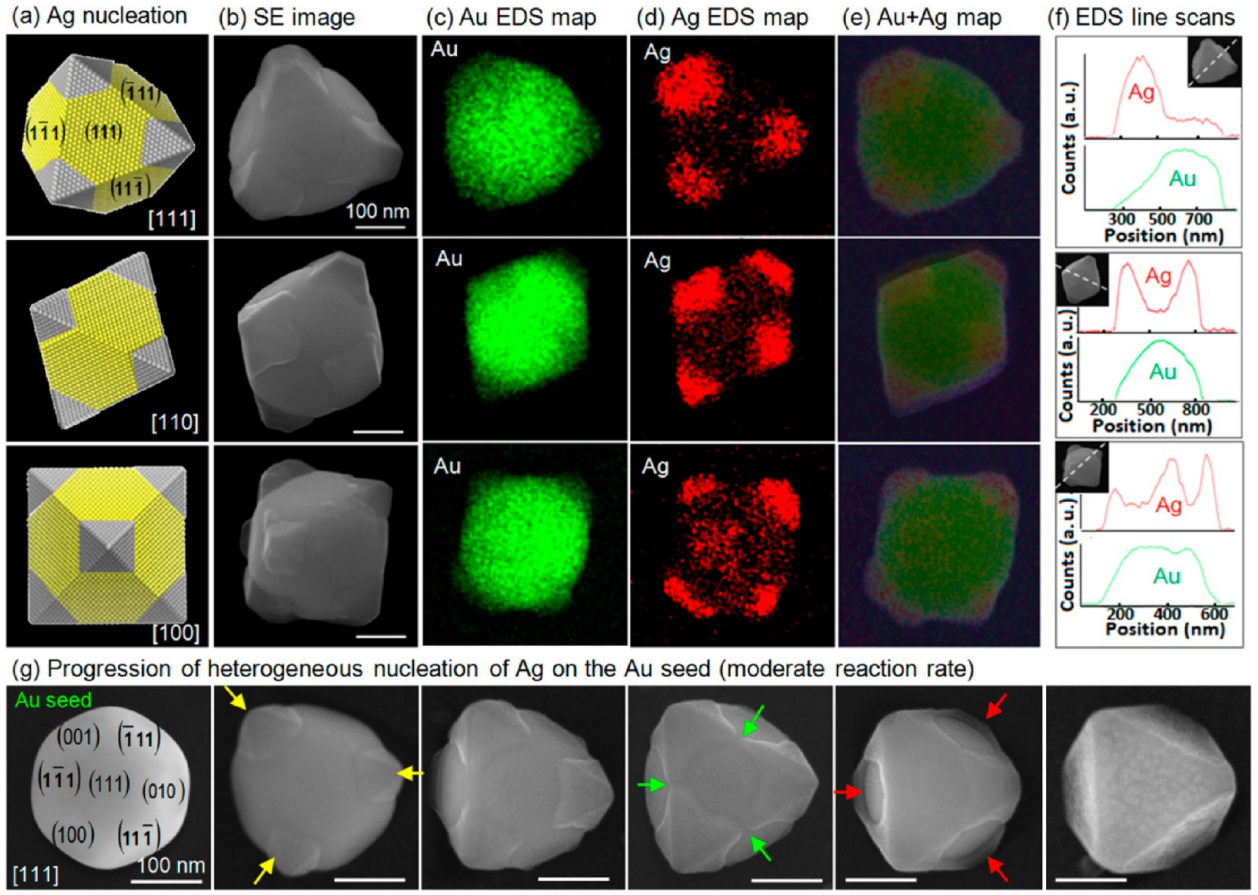

Figure 2. Early stage morphological and elemental characterization of bimetallic Au−Ag structures formed in the regime of moderate kinetics. (a) Schematic depictions of the topography expected for bimetallic structures formed after the deposition of Ag on the {100} facets of [111]-, [110]-, and [100]-oriented Au seeds. (b) SEM images of the structures formed in the early stages of the reaction and their corresponding (c) Au, (d) Ag, and (e) Au+Ag elemental maps and (f) line scans. (g) SEM images showing the early to late stage progression in morphology which reveals a Au seed being overgrown with Ag to the point of encapsulation.

geometry (Figure 1a) are exposed to the regime of slow kinetics. Figure 1b shows an SEM image of a periodic array of reacted seeds. Emerging from each of the truncated octahedrons is a structure which is either three- or six-fold symmetric (Figure 1c), geometries consistent with the largest facet being [111]-oriented. The overall faceting is consistent with either a hexagonal or truncated bipyramid geometry, structures which require the existence of a single planar twin boundary parallel to the largest [111] facet.[40] The triangle edge length/thickness ratio consistently lies in the range of 2:3. Noteworthy is that in no instance have we observed seeds which nucleate more than one of these structures. Images taken in electron backscattering mode (Figure 1d), elemental mapping (Figure 1e), and line scans (Figure 1f) all confirm the anisotropic deposition of Ag. The elemental mapping does, however, suggest that some alloying may occur at the Au−Ag interface and that a small amount of Ag is deposited over the entire Au seed. The nucleation site for both the triangular and hexagonal Ag structures is always one of the six {100} Au facets (Figure 1e). Strong evidence for a heteroepitaxial relationship at the nucleation site is provided by the fact that the [111] Ag facet for both the triangular and hexagonal geometries is always parallel to one of the {111} Au facets on the truncated octahedron. This geometrical relationship is highlighted by the labeled facets in Figure 1e, which show the (111) Ag facet being parallel to the $(1\bar{1}1)$ Au facet.

Bimetallic Structures Synthesized in the Regime of Moderate Kinetics. In the regime of moderate kinetics, Ag deposition initially occurs on the {100} Au facets of the truncated octahedron. The deposition occurs in a manner which replaces the exposed {100} Au facets with Ag pyramidal structures bound by {111} facets. The overall structure, therefore, trends toward an octahedral geometry. Figure 2 shows a schematic of the expected geometry and the corresponding SEM images, elemental maps, and line scans for bimetallic structures formed using [111]-, [110]-, and [100]-oriented Au seeds (note that the structures referred to as [100]-oriented are somewhat tilted off of the true [100] axes). While the structures in this regime show nearly identical Ag growth on all {100} Au facets (Figure 2b), it is noted that slightly slower reaction rates yield pyramidal structures with sharp corners, but where some of {100} facets are left unreacted (Supporting Information, Figure S2a). Slightly greater rates lead to structures with a mixture of sharp and blunt corners (Supporting Information, Figure S2b). The elemental maps and line scans for all three orientations (Figure 2c−f) show preferential Ag deposition on the {100} facets of the Au seed, with little deposition elsewhere. If, however, the reaction is allowed to proceed for longer times, the seed becomes completely overgrown with Ag. Figure 2g shows the progression observed as more and more Ag is deposited onto a [111]-oriented Au seed. After an initial stage, which sees the

dx.doi.org/10.1021/ja5081635 | J. Am. Chem. Soc. 2014, 136, 15337−15345

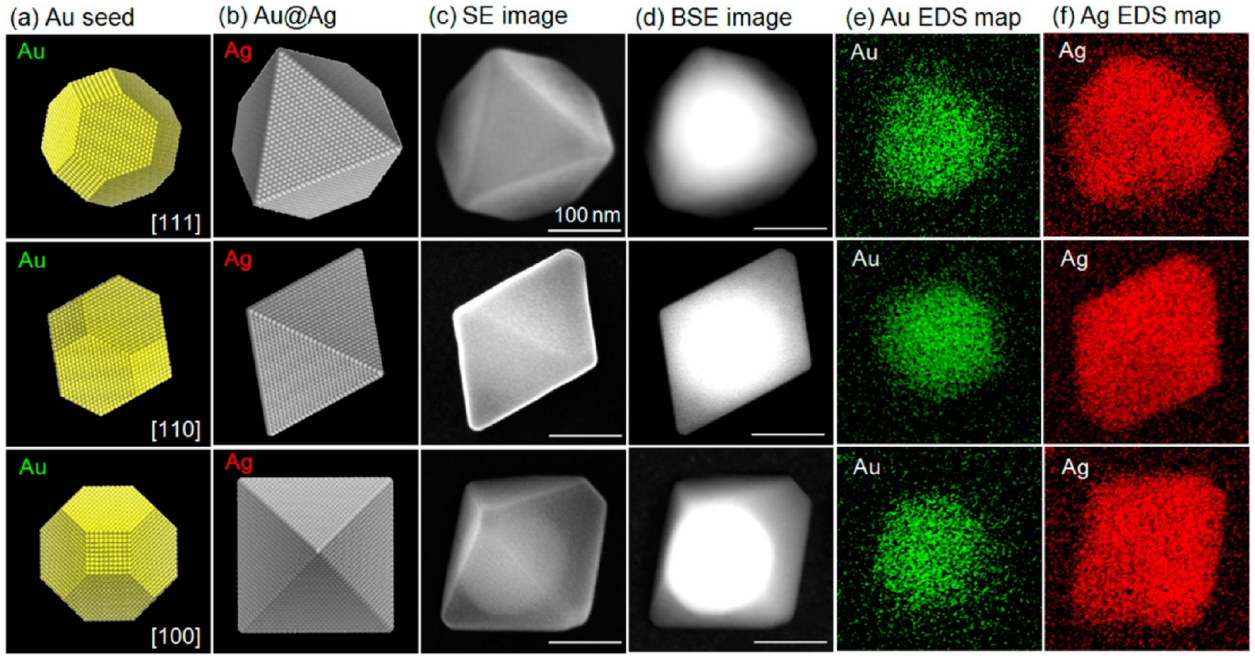

Figure 3. Late stage morphological and elemental characterization of bimetallic Au@Ag structures formed in the regime of moderate kinetics. Schematics of (a) [111]-, [110]-, and [100]-oriented Au seeds followed by (b) depictions of the Au@Ag structures formed in the late stages of the reaction. SEM images of the observed structures taken in (c) secondary electron and (d) backscatter modes and their corresponding (e) Au and (f) Ag elemental maps.

formation of Ag pyramids on the {100} Au facets (denoted by yellow arrows), Ag begins to deposit along the edges of the Au-truncated octahedron where the {111} Au facets meet (denoted by green arrows), a process which eventually leaves the {111} Au facets partially exposed and encircled by Ag (denoted by red arrows). Continued deposition results in the complete overgrowth of the exposed facets, forming an octahedron with Au@Ag geometry. Such structures are formed for all seed orientations. Figure 3a,b shows schematic representations of the [111]-, [110]-, and [100]-oriented Au seeds and the core−shell geometries expected after Ag overgrowth. SEM images taken in secondary electron mode show that these geometries are experimentally realized (Figure 3c). Backscatter mode images show the *Z*-contrast expected for Au@Ag structures (Figure 3d), a geometry which is confirmed by the Au and Ag elemental maps (Figure 3e,f).

Bimetallic Structures Synthesized in the Regime of Fast Kinetics. In the regime of fast kinetics, the Au seed becomes encapsulated with a far more uniform layer of Ag in a manner which, to a large extent, preserves the geometry of the initial seed. Figure 4a shows the progression in morphology which occurs as the Au seed is transformed into a Au@Ag structure. In contrast to the regime of moderate kinetics, early stage Ag deposition on the {100} facets does not lead to the formation of pyramid structures. Instead, the overgrowth is characterized by the simultaneous deposition of a relatively thin layer on the {100} facets (denoted by yellow arrows) and ridges of similar thickness along the edges of the truncated octahedron where the {111} Au facets meet (denoted by green arrows), a process which leaves the {111} Au facets partially exposed and encircled by Ag. Continued deposition results in a contraction of the exposed {111} facet area as a growth front advances to the point of complete seed encapsulation (denoted by red arrows). The final Au@Ag structure shows a geometry similar to that of the truncated octahedron. Figure 4b−g shows schematic representations, secondary electron and backscatter SEM images, elemental mapping, and line scans for the so-formed structures. The backscatter images confirm the core−shell morphology. Both the elemental mapping and line scans show that, while the overgrowth of Ag onto the Au seed is far more uniform than for the case of moderate kinetics, the lowest rate of deposition still occurs on the {111} Au facets. The Ag line scan for the [100] structure is particularly revealing in this regard as it passes through both the (1−11) and (010) facets but only shows a prominent peak for the (010) facet. Preferential deposition of Ag on the ridges where {111} Au facets meet is apparent from the line scan made over the [110]-oriented structure which shows a peak at each of the three positions corresponding to this feature.

Mechanistic Framework. The current study demonstrates that the site-selective heterogeneous nucleation and growth of Ag on Au seeds occurs even if the synthesis is surfactant-free. The slow regime, characterized by a single nucleation event, is quite revealing in that a layer-by-layer growth mode is inhibited off of the (100) Au facet where the nucleation occurs. Instead, an anisotropic Ag growth front propagates away from the seed into the adjacent solution. Also apparent is that the initial nucleation event is not one of low probability as all of the seeds are able to nucleate a single structure of approximately the same size. The nucleation of a second structure onto the same seed is, however, an extremely low probability event, a result whose implication is that the first nucleation event somehow inhibits subsequent nucleation events on the same Au seed. Similar behavior observed in the slow kinetic regime for other systems has been attributed to diffusion of atoms to the single nucleation site or the collision patterns between the seed and atoms in the liquid. These explanations, however, seem implausible for the much larger Ag structures produced in our syntheses (Figure 1c). Such structures, on average, require the addition of approximately 200 000 Ag atoms/s over the

dx.doi.org/10.1021/ja5081635 | *J. Am. Chem. Soc.* 2014, 136, 15337−15345

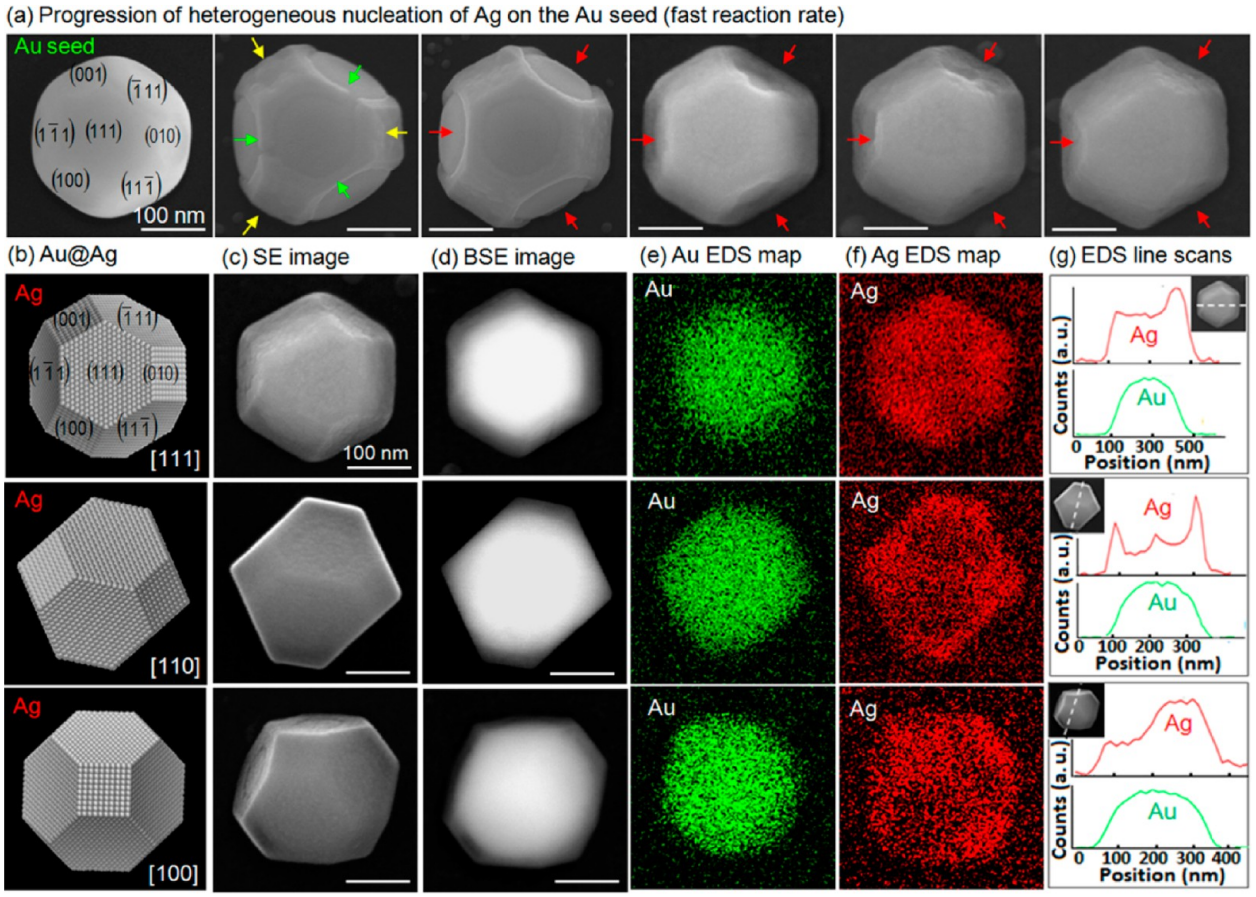

Figure 4. Morphological and elemental characterization of bimetallic Au@Ag structures formed in the regime of fast kinetics. (a) SEM images showing the observed progression in morphology where a Au seed is overgrown on its {100} facets followed by the overgrowth of its {111} facets to the point of encapsulation. (b) Schematic depictions of the topography expected for a [111]-, [110]-, and [100]-oriented structure derived from a growth mode which is dominated by the near uniform overgrowth of the {100} Au facets with Ag. SEM images of the observed structures taken in (c) secondary electron and (d) backscatter modes and their corresponding (e) Au and (f) Ag elemental maps and (g) line scans.

course of the 10 min synthesis. For surface diffusion to occur at these levels without other nucleation events occurring seems unlikely. Thermodynamic arguments also favor a surface diffusion which drives the system toward a geometry with a lower overall surface energy. This, however, is not the case because the final structure significantly increases the overall surface area, and Ag, because of its lower surface energy, should tend to wet Au rather than agglomerate on its surface. In an effort to further rule out surface diffusion as the predominant mass transport mechanism, Ag-topped Au pedestals (diameter 1.2 μm, 10 nm Ag, 50 nm Au) were deposited through a shadow mask and then exposed to 100 °C aqueous $AgNO_3$ for 10 min. If Ag diffusion on Au is significant and amenable to agglomeration under the reaction conditions, then significant Ag agglomeration should also occur on these pedestals. There is, however, no appreciable agglomeration observed (Supporting Information, Figure S3). Collision patterns also seem an unlikely candidate since liquid flow patterns are likely to be similar for adjacent seeds when immobilized in periodic arrays, yet no correlation between the Ag growth front directions for adjacent seeds is observed. We also contend that substrate influences are minimal in establishing this growth mode because sapphire, being an excellent insulator, is unlikely to offer an alternative pathway for electrons involved in the reactions. The fact that the kinetic regimes are similar to those observed when using solution-dispersed templates is supportive of this argument. We cannot, however, completely rule out possible substrate influences derived from its surface-altering liquid flows or through presenting a dielectric medium to the attached seeds. With these explanations seemingly unable to account for the current results, an alternative mechanistic framework (Figure 5) is required. While the Au seeds used in this study initially exhibit bare metallic surfaces, it should be recognized that their placement in a liquid media containing various reactants can dramatically alter this situation. In fact, numerous protocols exist where the synthesized single-component metallic nanostructures are stabilized against agglomeration, not by surfactants specifically added for this purpose, but by the reducing agents, solvents, or salts used in the synthesis.[41] Such protocols, while referred to as surfactant-free, still result in the formation of a stabilizing layer around each nanoparticle, but where the negative impact of this layer on catalytic properties,[42] photoluminescence,[43,44] and surface-enhanced Raman scattering sensitivities[45] is often significantly less than those of surfactants. On the basis of these supportive studies, we propose that such an interface layer is crucial in rationalizing the site-selective nature of our observed growth mode. With only two reactants, AA and $AgNO_3$, relatively few possibilities exist when trying to deduce the makeup of such an interface.

At the beginning of the synthesis, the Au seeds are inserted into a solution of solvated Ag^+ and NO_3^- ions where both the

dx.doi.org/10.1021/ja5081635 | J. Am. Chem. Soc. 2014, 136, 15337−15345

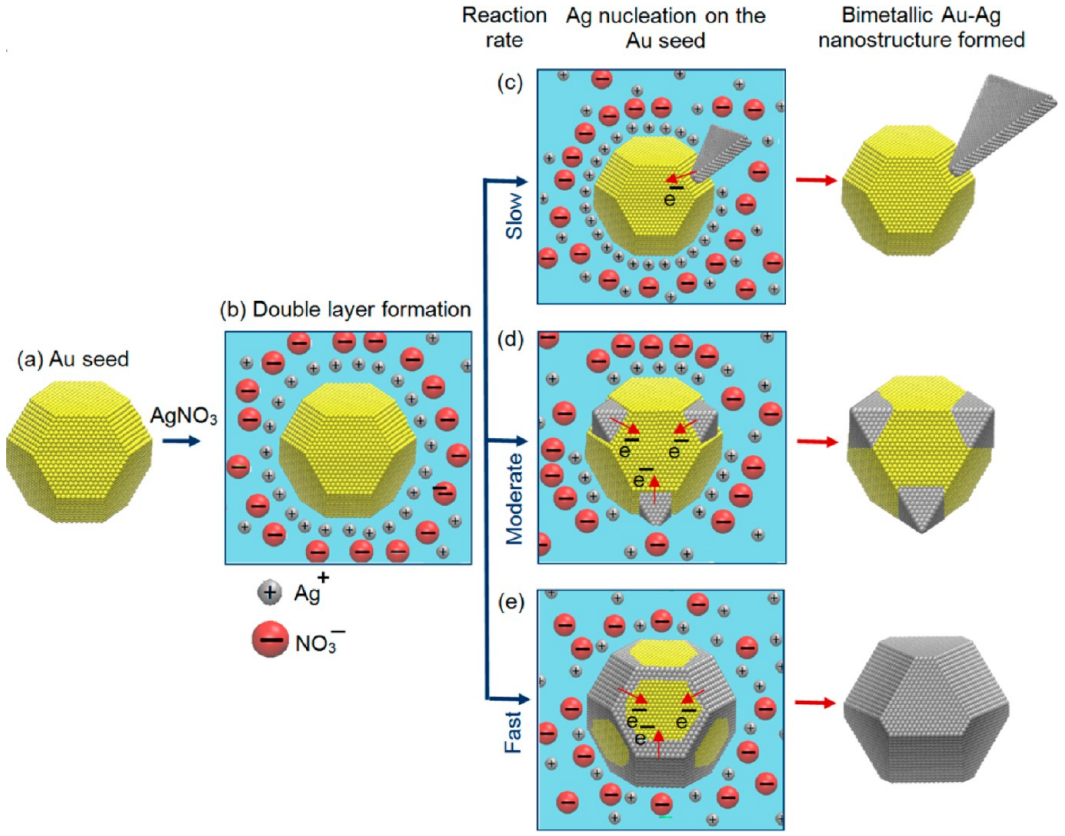

Figure 5. Schematic illustration of the mechanistic framework responsible for the heterogeneous nucleation of Ag on surfactant-free Au seeds. It shows (a) the initial seed, (b) the seed after double-layer formation and the progression of the reaction once the reducing agent is added in the (c) slow, (d) moderate, and (e) fast regimes.

positive and negative ion content is approximately 50 times greater than the number of Au atoms collectively contained within all the substrate-based seeds. Such a situation is very much analogous to the insertion of a metal electrode at zero potential into an electrolytic solution.[46] The resulting interaction can be described in terms of a simple jellium model which depicts a metal as an electron plasma interacting with positive ions represented by a continuous background. At the metal surface, the positive background falls abruptly to zero while the electron distribution extends slightly past this positive boundary. The exposure of this layer to the electrolytic solution leads to a situation where positive metal ions are attracted to the surface and attach either as a layer deposited at underpotential[47] or as a combination of solvated and specifically absorbed ions.[46] With the overall structure becoming positively charged, negative ions will be attracted to it, resulting in the formation of a space charge region consisting of a double layer of positive and negative ions (Figure 5b).[46] With various crystalline surfaces expressing different surface energies, the consistency of the space charge region is expected to fluctuate over the surface of the faceted metal seed, a property which can ultimately contribute to site-selective deposition. Evidence that such a layer exists for the current synthesis is the Ag detected in EDS measurements for the case where Au seeds are exposed to aqueous $AgNO_3$ and then removed from the solution without exposure to a reducing agent (Supporting Information, Figure S4).

For reduced Ag atoms to nucleate on a Au seed surrounded by an interfacial double layer, they must first displace the ions which make up this layer. For the slow regime (Figure 5c), nucleation occurs on a single {100} Au facet, but where layer-by-layer growth on the facet is inhibited. Such behavior is consistent with a double layer which is firmly affixed to the Au seed. With nucleation inhibited on the surface of Au, the growth front instead propagates toward the solution on Ag surfaces which are more amenable to deposition. To account for the fact that a second nucleation event does not occur on equivalent facets of the same Au seed, it must be recognized that the initial nucleation event results in the formation of a junction between neutrally charged Ag and a Au structure which is positively charged due the ions which attached to its surface. Such a scenario is conducive to electron transfer from Ag to Au. The electrons added to Au will, in turn, increase the attractive force which binds the double layer to the Au structure and, hence, inhibit the nucleation of Ag on other {100} facets. Reaction rates in the moderate and fast regime (Figure 5d,e), facilitated by the fast injection of AA, not only give rise to faster kinetics but also result in a rapid decrease in the pH of the solution (compared to the slow decrease resulting from a dropwise injection). Faster kinetics can lead to the near simultaneous nucleation of Ag at multiple sites on the structures while the increase in pH can fundamentally alter the nature of the double layer surrounding each of the Au structures. If, under these circumstances, the ions forming the double layer are more readily displaced by Ag^0, it would account for the layer-by-layer growth observed on each of the {111} Au facets and the eventual overgrowth of the entire seed with Ag.

dx.doi.org/10.1021/ja5081635 | J. Am. Chem. Soc. 2014, 136, 15337−15345

CONCLUSIONS

In summary, we have demonstrated the heterogeneous nucleation of Ag on substrate-based Au seeds in a surfactant-free aqueous medium. Despite the fact that the synthesis is unperturbed by surfactants, the deposition remains anisotropic and strongly dependent on whether the reaction is carried out in a regime of slow, moderate, or fast kinetics. Slow kinetics give rise to a Au−Ag bimetallic heterodimer obtained through epitaxial deposition on just a small portion of a single {100} Au facet followed by the propagation of a rapid growth front away from the seed into the liquid medium. Moderate kinetics result in a Au@Ag structure with an octahedron geometry realized through layer-by-layer deposition of Ag on all {100} equivalent seed facets followed by the overgrowth of all remaining facets. Fast kinetics also result in a core−shell morphology, where the overgrowth more closely follows the topography of the underlying seed. Our understanding of various regimes requires the formation of a facet-dependent space charge region around the seed which is responsive to the injection of electrons from the deposited Ag layer as well as the concentration of ascorbic acid within the solution. Taken together, the work demonstrates that even the simplest of seed-mediated protocols involving heterogeneous nucleation gives rise to unexpectedly rich phenomenology.

ASSOCIATED CONTENT

Supporting Information

Additional data are provided which shows (i) SEM images and an accompanying histogram showing Au seed uniformity, (ii) SEM images of bimetallic structures synthesized using reaction rates which are somewhat slower and faster than those used in the regime of moderate kinetics, (iii) data demonstrating that no appreciable Ag agglomeration occurs when deposited on Au pedestals and exposed to aqueous $AgNO_3$ at boiling temperatures, and (iv) EDS data showing that a Ag signature is apparent when Au seeds are exposed to aqueous $AgNO_3$ and then removed from the solution without exposure to ascorbic acid. This material is available free of charge via the Internet at http://pubs.acs.org.

AUTHOR INFORMATION

Corresponding Author

neretina@temple.edu

Notes

The authors declare no competing financial interest.

ACKNOWLEDGMENTS

This work is funded by the NSF (DMR-1053416) CAREER Award to S.N. The authors also acknowledge the expertise of D. Dikin (Facility Manager, Nano Instrumentation Center, Temple University). The work has benefited from the facilities available through Temple University's Material Research Facility (MRF). K.D.G. acknowledges support received through a Temple University Graduate Student Fellowship.

REFERENCES

(1) Wiley, B.; Sun, Y.; Chen, J.; Cang, H.; Li, Z.-Y.; Li, X.; Xia, Y. *MRS Bull.* **2005**, *30*, 356−361.
(2) Grzelczak, M.; Perez-Juste, J.; Mulvaney, P.; Liz-Marzan, L. M. *Chem. Soc. Rev.* **2008**, *37*, 1783−1791.
(3) Carbone, L.; Cozzoli, P. D. *Nano Today* **2010**, *5*, 449−493.
(4) Lim, B.; Jiang, M.; Camargo, P. H. C.; Cho, E. C.; Tao, J.; Lu, X.; Zhu, Y.; Xia, Y. *Science* **2009**, *324*, 1302−1305.
(5) Mazumder, V.; Chi, M.; Mankin, M. N.; Liu, Y.; Metin, O.; Sun, D.; More, K. L.; Sun, S. *Nano Lett.* **2012**, *12*, 1102−1106.
(6) Holewinski, A.; Xin, H.; Nikolla, E.; Linic, S. *Curr. Opin. Chem. Eng.* **2013**, *2*, 312−319.
(7) Cui, C.; Yu, J.; Li, H.; Gao, M.; Liang, H.; Yu, S. *ACS Nano* **2011**, *5*, 4211−4218.
(8) Sneed, B. T.; Young, A. P.; Golden, M. C.; Mao, S.; Jiang, Y.; Wang, Y.; Tsung, C. K. *ACS Nano* **2014**, *8*, 7239−7250.
(9) Kelly, K. L.; Coronado, E.; Zhao, L. L.; Schatz, G. C. *J. Phys. Chem. B* **2003**, *107*, 668−677.
(10) Atwater, H. A.; Polman, A. *Nat. Mater.* **2010**, *9*, 205−213.
(11) Huang, J.; Zhu, Y.; Lin, M.; Wang, Q.; Zhao, L.; Yang, Y.; Yao, K. X.; Han, Y. *J. Am. Chem. Soc.* **2013**, *135*, 8552−8561.
(12) Nasir, M. E.; Dickson, W.; Wurtz, G. A.; Wardley, W. P.; Zayats, A. V. *Adv. Mater.* **2014**, *26*, 3532−3537.
(13) Chatterjee, K.; Sarkar, S.; Rao, K. J.; Paria, S. *Adv. Colloid Interface Sci.* **2014**, *209*, 8−39.
(14) Hao, R.; Xing, R.; Xu, Z.; Hou, Y.; Gao, S.; Sun, S. *Adv. Mater.* **2010**, *22*, 2729−2742.
(15) Griffith, R. G.; Hommer, M. B.; Grabar, K. C.; Jackson, M. A.; Natan, M. J. *J. Phys. Chem.* **1996**, *100*, 718−724.
(16) Rivas, L.; Sanchez-Cortes, S.; Garcia-Ramos, J. V.; Morcillo, G. *Langmuir* **2000**, *16*, 9722−9728.
(17) Cao, Y. W.; Jin, R.; Mirkin, C. A. *J. Am. Chem. Soc.* **2001**, *123*, 7961−7962.
(18) Moskovits, M.; Srnová-Šloufová, I.; Vlčková, B. *J. Chem. Phys.* **2002**, *116*, 10435−10446.
(19) Sanedrin, R. G.; Georganopoulou, D. G.; Park, S.; Mirkin, C. A. *Adv. Mater.* **2005**, *17*, 1027−1031.
(20) Habas, S. E.; Lee, H.; Radmilovic, V.; Somorjai, G. A.; Yang, P. *Nat. Mater.* **2007**, *6*, 692−697.
(21) Fan, F. R.; Liu, D. Y.; Wu, Y. F.; Duan, S.; Xie, Z. X.; Jiang, Z. Y.; Tian, Z. Q. *J. Am. Chem. Soc.* **2008**, *130*, 6949−6951.
(22) Yang, Y.; Zhang, Q.; Fu, Z. W.; Qin, D. *ACS Appl. Mater. Interfaces* **2014**, *6*, 3750−3757.
(23) Yang, Y.; Liu, J.; Fu, Z. W.; Qin, D. *J. Am. Chem. Soc.* **2014**, *136*, 8153−8156.
(24) Lee, H.; Habas, S. E.; Somorjai, G. A.; Yang, P. *J. Am. Chem. Soc.* **2008**, *130*, 5406−5407.
(25) Lim, B.; Kobayashi, H.; Yu, T.; Wang, J.; Kim, M. J.; Li, Z. Y.; Rycenga, M.; Xia, Y. *J. Am. Chem. Soc.* **2010**, *132*, 2506−2507.
(26) Yang, Y.; Wang, W.; Li, X.; Chen, W.; Fan, N.; Zou, C.; Chen, X.; Xu, X.; Zhang, L.; Huang, S. *Chem. Mater.* **2013**, *25*, 34−41.
(27) Zhu, C.; Zeng, J.; Tao, J.; Johnson, M.; Schmidt-Krey, I.; Blubaugh, L.; Zhu, Y.; Gu, Z.; Xia, Y. *J. Am. Chem. Soc.* **2012**, *134*, 15822−15831.
(28) Xie, S.; Peng, H.-C.; Lu, N.; Wang, J.; Kim, M. J.; Xie, Z.; Xia, Y. *J. Am. Chem. Soc.* **2013**, *135*, 16658−16667.
(29) Tao, A. R.; Habas, S.; Yang, P. *Small* **2008**, *4*, 310−325.
(30) Murphy, C. J.; Sau, T. K.; Gole, A. M.; Orendorff, C. J.; Gao, J.; Gou, L.; Hunyadi, S. E.; Li, T. *J. Phys. Chem. B* **2005**, *109*, 13857−13870.
(31) Fievet, F.; Lagier, J. P.; Figlarz, M *MRS Bull.* **1989**, *14*, 29−34.
(32) Selvakannan, P. R.; Swami, A.; Srisathiyanarayanan, D.; Shirude, P. S.; Pasricha, R.; Mandale, A. B.; Sastry, M. *Langmuir* **2004**, *20*, 7825−7836.
(33) Gilroy, K. D.; Farzinpour, P.; Sundar, A.; Tan, T.; Hughes, R. A.; Neretina. *Nano Res.* **2013**, *6*, 418−428.
(34) Gilroy, K. D.; Sundar, A.; Farzinpour, P.; Hughes, R. A.; Neretina, S. *Nano Res.* **2014**, *7*, 365−379.
(35) Gilroy, K. D.; Farzinpour, P.; Sundar, A.; Hughes, R. A.; Neretina, S. *Chem. Mater.* **2014**, *26*, 3340−3347.
(36) Thompson, C. V. *Annu. Rev. Mater. Res.* **2012**, *42*, 399−434.
(37) Farzinpour, P.; Sundar, A.; Gilroy, K. D.; Eskin, Z. E.; Hughes, R. A.; Neretina, S. *Nanoscale* **2013**, *5*, 1929−1938.
(38) Farzinpour, P.; Sundar, A.; Gilroy, K. D.; Eskin, Z. E.; Hughes, R. A.; Neretina, S. *Nanotechnology* **2012**, *23*, 495604.

(39) Henry, C. R. *Prog. Surf. Sci.* **2005**, *80*, 92−116.
(40) Zhang, J.; Langille, M. R.; Mirkin, C. A. *J. Am. Chem. Soc.* **2010**, *132*, 12502−12510.
(41) Kawasaki, H. *Nanotechnol. Rev.* **2013**, *2*, 5−25.
(42) Niu, Z.; Li, Y. *Chem. Mater.* **2014**, *26*, 72−83.
(43) Liu, X. F.; Li, C. H.; Xu, J. L.; Lv, J.; Zhu, M.; Guo, Y. B.; Cui, S.; Liu, H. B.; Wang, S.; Li, Y. L. *J. Phys. Chem. C* **2008**, *112*, 10778−10783.
(44) Kawasaki, H.; Yamamoto, H.; Fujimori, H.; Arakawa, R.; Inada, M.; Iwasaki, Y. *Chem. Commun.* **2010**, *46*, 3759−3761.
(45) Dar, M. I.; Sampath, S.; Shivashankar, S. A. *J. Mater. Chem.* **2012**, *22*, 22418−22423.
(46) Schmickler, W.; Santos, E. *Interfacial Electrochemistry*, 2nd ed.; Springer: Berlin, 2010.
(47) Herrero, E.; Buller, L. J.; Abruña, H. D. *Chem. Rev.* **2001**, *101*, 1897−1930.